FERMILAB-PUB-12-518-CD

Impedances and wake functions for non-ultrarelativistic beams in circular chambers

Alexandru Macridin, Panagiotis Spentzouris, James Amundson
Fermilab, P.O. Box 500, Batavia, Illinois 60510, USA

We obtain general expressions for the longitudinal and the transverse impedances in circular chambers, valid for all types of walls as long as the wall surface impedance can be defined. We numerically calculate the resistive-wall wakes for metallic and laminated chambers and discuss the validity of the ultrarelativistic approximation for non-ultrarelativistic beams. We find that the ultrarelativistic approximation fails to describe the wake effects at distance smaller than ≈ 0.1 m for chambers with radius of a few centimeters at small and intermediate γ. In this small distance region, the non-ultrarelativistic wake is nonzero ahead of the source and is strongly overestimated by the ultrarelativistic approximation behind the source. Non-ultrarelativistic beams yield transverse wake terms which couple with the displacement of both the source and the affected particles. The latter wake term is of order $\mathcal{O}(\gamma^{-2})$ and acts in the small distance region both ahead of and behind the source.

I. INTRODUCTION

Wakefields are a leading cause of losses and instabilities in high intensity accelerators. The calculation of non-ultrarelativistic wakefields and impedances is of major importance since there are a large number of machines, especially at the beginning of the acceleration cycle, which run beams with velocity significantly smaller than the speed of light.

There is a vast literature addressing the calculation of wakefields and impedances in accelerators, see for example Ref. [1–3] and references therein. Most of the studies consider ultrarelativistic beams. Nevertheless, in the recent years, a number of papers have recognized the importance of non-ultrarelativistic effects [3–9]. These papers calculate the monopole longitudinal and the dipole transverse impedance for metallic or multilayer circular chambers. General expressions for the impedance in multilayer chambers are calculated in Ref [8, 9]. Approximate analytical expressions for the metallic chamber wake functions are given in [5].

In this paper we provide general expressions for longitudinal and transverse impedances in circular chambers, valid for all types of walls as long as the wall surface impedance can be defined. While in most of the previous investigations the impedance is expressed as function of wall conductivity or skin penetration depth, we express our results as function of wall surface impedance. Similar expressions for the impedance as function of wall surface impedance are also given by Hahn [9]. The wall's electrical properties are contained implicitly in the wall surface impedance which can be determined separately for each specific problem and does not constitute the subject of this paper. In many cases, such as the thick metallic wall [10, 11], thin metallic wall [10], multilayered wall [9] or laminated structure [12] the wall surface impedance is already known. For example, by plugging into our equations the laminated chamber surface impedance, we can immediately calculate the non-ultrarelativistic impedance for laminated structures. Note that, since the laminated chambers walls are not made by a continuum electrical medium characterized by a well defined conductivity, the formalism of [4–8] cannot be applied in this case. We find that, in addition to the longitudinal impedance, the monopole channel also yields a transverse impedance. This term, which vanishes in the ultrarelativistic limit, had not previously appeared in the literature to our knowledge.

Complex numerical simulations require the knowledge of the space-time wake functions rather than of the frequency-dependent impedance. It is especially useful to have the resistive-wall wakes which originate only from the the wall finite resistivity, since in most algorithms (SYNERGIA [13], IMPACT [14], ORBIT [15]) the direct space charge wake and the wake originating from the ideal image charges and currents are already implemented by employing sophisticated Poisson solvers. The resistive-wall wakes are exactly the extra effects which should be added to these simulations. Here we numerically calculate the resistive-wall wake functions for metallic and laminated chambers, then investigate the validity of the ultrarelativistic approximation for non-ultrarelativistic beams.

We find that the ultrarelativistic approximation to non-ultrarelativistic beams fails to accurately describe wake effects at distances smaller than ≈ 0.1 m for chambers with radius of a few centimeters for small and intermediate γ. This small distance region, which is roughly proportional to $\frac{b}{\gamma}$, extends both ahead of and behind the source. Unlike the ultrarelativistic wake, which vanishes in front of the source, we find for the non-ultrarelativistic case a repulsive wake ahead of the source, a consequence of the fact that the electromagnetic field propagates faster than the source itself. In the small distance region behind the source, the ultrarelativistic approximation strongly overestimates the wake fields. Aside from the familiar transverse wake term which couple to the source particle displacement, non-ultrarelativistic beams in circular chambers are also characterized by a transverse wake which couples with the displacement of the affected particle. This transverse wake term is $\mathcal{O}(\gamma^{-2})$ and acts in the small distance region both

Operated by Fermi Research Alliance, LLC under Contract No. De-AC02-07CH11359 with the United States Department of Energy.

ahead of and behind the source.

The paper is organized as follows. In Sec.II we introduce the general definitions of the quantities used throughout the paper. The longitudinal and transverse impedances and wakes are calculated in Sec.III. The validity of the ultrarelativistic approximation is also discussed in this section. We end with a summary and conclusions in Sec.IV.

II. GENERAL FORMALISM

The wake functions describe the effect of the electromagnetic field created by a particle moving through an accelerator beam pipe upon the other particles in the beam. Consider a beam flowing with velocity βc along the z-direction in a circular pipe. If the distance between the source and the affected particle is z, the momentum of the affected particle traversing a structure of length L will be modified by [16, 17]:

$$\beta c \Delta p_z = -qQW_0^{||}(z) \tag{1}$$
$$\beta c \Delta p_x = -qQ(W_1^{\perp}(z)X + W_0^{\perp}(z)x) \tag{2}$$
$$\beta c \Delta p_y = -qQ(W_1^{\perp}(z)Y + W_0^{\perp}(z)y) \ . \tag{3}$$

Here Q (q) and (X, Y) ((x, y)) represent the charge and transverse displacement of the source (affected) particle respectively. $||$ and $\perp$ denote the longitudinal and the transverse directions. The higher-order terms in the displacement are neglected.

Note that, in the ultrarelativistic limit, the second term describing the transverse kick proportional to the affected particle displacement, $W_0^{\perp}$, is zero. For non-ultrarelativistic beams, as it will be shown, it is of order $\mathcal{O}(\gamma^{-2})$.

The impedance and the wake functions are related via Fourier transforms,

$$W_0^{||}(z) = \frac{1}{2\pi}\int_{-\infty}^{\infty} d\omega Z_0^{||}(\omega) e^{-j\frac{\omega}{\beta c}z} \tag{4}$$
$$W_{0,1}^{\perp}(z) = \frac{j}{2\pi}\int_{-\infty}^{\infty} d\omega Z_{0,1}^{\perp}(\omega) e^{-j\frac{\omega}{\beta c}z} \ . \tag{5}$$

It is convenient to distinguish two different contributions to the wake field

$$W = W^{\infty} + W^{\sigma} \ . \tag{6}$$

W^{∞} is due to the direct space charge contribution together with the contribution of the image charges and image currents in the wall as if the wall were a perfect conductor, and is obtained by setting the wall resistivity to zero. W^{σ} is the resistive-wall wake due to the wall's finite resistivity. This separation is especially useful in complex numerical beam dynamics simulations. In most codes [13–15] W^{∞} is already taken into account by considering the effects of the electromagnetic field obtained by numerically solving the Poisson equation in chambers with ideally conducting walls. The remaining contribution of the wake field, described by the resistive-wall wake W^{σ}, has to be incorporated separately.

We are going to derive the impedance functions by solving the Maxwell's equations in the frequency domain and then obtain the wake functions via Fourier transforms. Because one of the main goals of this paper is to address the validity of using the ultrarelativistic impedance in the calculation of the non-ultrarelativistic wake function, we define, for the purpose of comparison,

$$\tilde{W}_0^{||}(z,\gamma) = \frac{1}{2\pi}\int_{-\infty}^{\infty} d\omega Z_0^{||}(\omega, \gamma = \infty) e^{-j\frac{\omega}{\beta c}z} \tag{7}$$
$$\tilde{W}_{0,1}^{\perp}(z,\gamma) = \frac{j}{2\pi}\int_{-\infty}^{\infty} d\omega \beta Z_{0,1}^{\perp}(\omega, \gamma = \infty) e^{-j\frac{\omega}{\beta c}z} \ . \tag{8}$$

Thus the ultrarelativistic approximate wake function $\tilde{W}$ is obtained after a Fourier transform with the modulation factor $e^{-j\frac{\omega}{\beta c}z}$ of the ultrarelativistic impedance. In the definition of the transverse wake $\tilde{W}^{\perp}$ an additional factor of β is included in front of the ultrarelativistic impedance, since in the first order the transverse impedance at finite γ is approximated with the ultrarelativistic impedance multiplied by a factor of β [18].

The electromagnetic field is related to the electric potential Φ and the magnetic vector potential $\vec{A}$ by

$$\vec{E} = -\nabla\Phi - \frac{\partial \vec{A}}{\partial t} \tag{9}$$
$$Z_0\vec{H} = c\nabla \times \vec{A} \ , \tag{10}$$

where Φ and $\vec{A}$ satisfy

$$\nabla^2\phi - \frac{1}{c^2}\frac{\partial^2\Phi}{\partial t^2} = -\frac{\rho}{\epsilon_0} \tag{11}$$

$$\nabla^2\vec{A} - \frac{1}{c^2}\frac{\partial^2\vec{A}}{\partial t^2} = -\mu_0\vec{j} \tag{12}$$

$$\nabla\vec{A} + \frac{1}{c^2}\frac{\partial\phi}{\partial t} = 0 \ . \tag{13}$$

Eq. 13 is the Lorentz gauge condition. The potentials can undergo a gauge transformation

$$\vec{A}' = \vec{A} - \nabla\chi \tag{14}$$

$$\Phi' = \Phi + \frac{\partial\chi}{\partial t} \tag{15}$$

where the gauge field should satisfy

$$\nabla^2\chi - \frac{1}{c^2}\frac{\partial^2\chi}{\partial t^2} = 0 \ . \tag{16}$$

The source charge and current are moving along the z-direction with velocity βc. Thus

$$\rho, j_z \propto \delta(z - \beta ct) \propto e^{j(\omega t - kz)} \tag{17}$$

where $k = \frac{\omega}{\beta c}$. We are looking for synchronous solutions

$$\vec{E}(x,y,z,t) = \vec{E}(x,y)e^{j(\omega t - kz)} \tag{18}$$

$$\vec{H}(x,y,z,t) = \vec{H}(x,y)e^{j(\omega t - kz)} \ . \tag{19}$$

The longitudinal (transverse) impedance is proportional to the longitudinal (transverse) force acting on the affected particle. According to the definition of the wake function in Eq. 1 (Eqs. 2, 3) it should be defined as

$$Z_0^{||}(\omega) = -\frac{E_z^\sigma(\omega)|_{X,Y,x,y=0}}{Q\beta c} \tag{20}$$

$$Z_0^{\perp}(\omega) = -\frac{\frac{\partial F_x}{\partial x}(\omega)|_{X,Y,x,y=0}}{jqQ\beta c} \tag{21}$$

$$Z_1^{\perp}(\omega) = -\frac{\frac{\partial F_x}{\partial X}(\omega)|_{X,Y,x,y=0}}{jqQ\beta c} \ . \tag{22}$$

where F_x is the transverse Lorentz force along x direction acting on the affected particle.

The calculation of the impedance reduces to the calculation of the electromagnetic field inside the vacuum chamber. The electromagnetic field is determined by the boundary conditions at the chamber walls. In general this also requires the calculation of the field inside the walls and then imposing the field continuity conditions at the wall boundary, at is done in [4–8]. We find it convenient to express the field inside the vacuum chamber as function of the surface wall impedances. The surface wall impedances are defined as ratios of the transverse electric field and the transverse magnetic field at the wall. Of course, the calculation of the surface wall impedances requires the calculation of the field inside the wall. However, the advantage is that we separate the problem into two distinct parts. The first part, which is the focus of this paper, is to write the impedance as function of the wall surface impedance. This part does not care about the wall's electrical properties; it only assumes a chamber with circular geometry. The second part is the calculation of the wall surface impedance, which can be addressed separately for each specific problem. However, for many types of accelerator chambers (e.g. thick metallic wall [10], thin metallic wall [10], layered wall [9], laminated wall [12], etc.) there are well known solutions for the surface impedance which can just be plugged in the wake formalism described in this paper.

III. CALCULATION OF THE IMPEDANCE AND THE WAKE

Consider a particle which moves through a circular chamber of radius b with an offset $r = a$ in the $\Theta = 0$ direction from the central axis. In cylindrical coordinates, (r, θ, z), the charge density can be written as [19]

$$\rho(r,\theta,z,t) = \sum_{m=0} \rho_m \frac{\delta(r-a)}{a} \cos m\theta \ e^{j(\omega t - kz)} \tag{23}$$

where

$$\rho_m = \frac{I_m}{\pi a^m (1+\delta_{m,0})} \tag{24}$$

$$I_m = \rho a^m = Q a^m \ . \tag{25}$$

The potentials can be written as

$$[\phi(r,\theta,z,t), A_r(r,\theta,z,t), A_z(r,\theta,z,t)] = \sum_{m=0} [\phi_m(r), A_{rm}(r), A_{zm}(r)] \cos m\theta \ e^{j(\omega t - kz)} \tag{26}$$

$$A_\theta(r,\theta,z,t) = \sum_{m=0} A_{\theta m}(r) \sin m\theta \ e^{j(\omega t - kz)} \ . \tag{27}$$

For a particular multipole moment number m, the equations 11, 12, 13 become

$$\frac{d^2\phi}{dr^2} + \frac{1}{r}\frac{d\phi}{dr} - \left(\frac{m^2}{r^2} + k_r^2\right)\phi = -\frac{\rho_m}{\epsilon_0}\frac{\delta(r-a)}{a} \tag{28}$$

$$\frac{d^2A_r}{dr^2} + \frac{1}{r}\frac{dA_r}{dr} - \left(\frac{m^2+1}{r^2} + k_r^2\right)A_r - \frac{2m}{r^2}A_\theta = 0 \tag{29}$$

$$\frac{d^2A_\theta}{dr^2} + \frac{1}{r}\frac{dA_\theta}{dr} - \left(\frac{m^2+1}{r^2} + k_r^2\right)A_\theta - \frac{2m}{r^2}A_r = 0 \tag{30}$$

$$\frac{d^2A_z}{dr^2} + \frac{1}{r}\frac{dA_z}{dr} - \left(\frac{m^2}{r^2} + k_r^2\right)A_z = -\frac{\beta}{c}\frac{\rho_m}{\epsilon_0}\frac{\delta(r-a)}{a} \tag{31}$$

with $k_r = \frac{k}{\gamma}$, where for clarity we drop the subscript m for the potentials. The Lorentz gauge reads

$$\frac{dA_r}{dr} + \frac{A_r}{r} + \frac{m}{r}A_\theta - jk\left(A_z - \frac{\beta}{c}\phi\right) = 0 \ , \tag{32}$$

while gauge fields obeys

$$\frac{d^2\chi}{dr^2} + \frac{1}{r}\frac{d\chi}{dr} - \left(\frac{m^2}{r^2} + k_r^2\right)\chi = 0 \ . \tag{33}$$

The general solution for the homogeneous equation of type Eq. 33 is

$$\chi(r) = c_1 K_m(k_r r) + c_2 I_m(k_r r) \ , \tag{34}$$

where I_m and K_m are the modified Bessel functions of the first and the second kind, respectively, and of order m. c_1 and c_2 are arbitrary constants.

The electric and magnetic fields can be expanded as

$$[E_r(r,\theta,z,t), E_z(r,\theta,z,t), H_\theta(r,\theta,z,t)] = \sum_{m=0} [E_{rm}(r), E_{zm}(r), H_{\theta m}(r)] \cos m\theta \ e^{j(\omega t - kz)} \tag{35}$$

$$[E_\theta(r,\theta,z,t), H_r(r,\theta,z,t), H_z(r,\theta,z,t)] = \sum_{m=0} [E_{\theta m}(r), H_{rm}(r), H_{zm}(r)] \sin m\theta \ e^{j(\omega t - kz)} \ . \tag{36}$$

By again omitting the subscript m, one has

$$E_r = -\frac{d\phi}{dr} - jk\beta c A_r \tag{37}$$

$$E_\theta = \frac{m}{r}\phi - jk\beta c A_\theta \tag{38}$$

$$E_z = jk\left(\phi - \beta c A_z\right) \tag{39}$$

$$Z_0 H_r = c\left(\frac{m}{r}A_z + jkA_\theta\right) \tag{40}$$

$$Z_0 H_\theta = c\left(-jkA_r - \frac{dA_z}{dr}\right) \tag{41}$$

$$Z_0 H_z = c\left(\frac{dA_\theta}{dr} + \frac{A_\theta}{r} + \frac{m}{r}A_r\right) \ . \tag{42}$$

The transverse Lorentz forces are

$$\frac{F_r}{q} = E_r - \beta Z_0 H_\theta = -\frac{d}{dr}\left(\Phi - \beta c A_z\right) = j\frac{1}{k}\frac{dE_z}{dr} \tag{43}$$

$$\frac{F_\theta}{q} = E_\theta + \beta Z_0 H_r = \frac{m}{r}(\Phi - \beta c A_z) = -j\frac{m}{k}\frac{E_z}{r} \ . \tag{44}$$

In the following sections we are going to separately treat the monopole (i.e. $m = 0$) and dipole (i.e. $m = 1$) cases. The higher-order multipole channels yield wake effects of second or higher order in the particle displacement which are beyond the scope of this investigation.

A. Monopole channel, $m = 0$

1. *Electromagnetic field solution*

In this channel $A_\theta \propto \sin m\theta = 0$. The potentials satisfy

$$\frac{d^2\phi}{dr^2} + \frac{1}{r}\frac{d\phi}{dr} - k_r^2\phi = -\tfrac{\rho}{2\pi\epsilon_0}\tfrac{\delta(r-a)}{a} \tag{45}$$

$$\frac{d^2A_r}{dr^2} + \frac{1}{r}\frac{dA_r}{dr} - \left(\frac{1}{r^2} + k_r^2\right)A_r = 0 \tag{46}$$

$$A_\theta = 0 \tag{47}$$

$$\frac{d^2A_z}{dr^2} + \frac{1}{r}\frac{dA_z}{dr} - k_r^2 A_z = -\tfrac{\beta}{c}\tfrac{\rho}{2\pi\epsilon_0}\tfrac{\delta(r-a)}{a} \tag{48}$$

$$\frac{dA_r}{dr} + \frac{A_r}{r} - jk\left(A_z - \frac{\beta}{c}\phi\right) = 0 \ . \tag{49}$$

The radial component of the vector potential A_r is

$$A_r(r) = c_1 K_1(k_r r) + c_2 I_1(k_r r) \ . \tag{50}$$

By applying a gauge transformation with $\chi = -\frac{c_1}{k_r}K_0(k_r r) + \frac{c_2}{k_r}I_0(k_r r)$, and using the Bessel functions properties $K_0' = -K_1$ and $I_0' = I_1$, one can set $A_r = 0$. The Lorentz condition, Eq. 49, becomes

$$A_z = \frac{\beta}{c}\phi \ . \tag{51}$$

In order to determine the electric potential ϕ, note that the solution to the equation

$$\frac{d^2G_0}{dr^2} + \frac{1}{r}\frac{dG_0}{dr} - k_r^2 G_0 = -\frac{\delta(r-a)}{a} \tag{52}$$

is

$$G_0(r,a) = \begin{cases} K_0(k_r a)I_0(k_r r), & r < a \\ I_0(k_r a)K_0(k_r r), & r \geq a \ . \end{cases} \tag{53}$$

The justification uses the Bessel functions wronskian properties

$$I_0(x)K_0'(x) - I_0'(x)K_0(x) = \frac{1}{x} \tag{54}$$

and is similar to the one given in [3].

The solution for the potentials is therefore

$$\phi(r) = \frac{\rho}{2\pi\epsilon_0}G_0(r,a) + a_0 I_0(k_r r) \tag{55}$$

$$A_r(r) = 0 \tag{56}$$

$$A_\theta(r) = 0 \tag{57}$$

$$A_z(r) = \frac{\beta}{c}\phi(r) \ . \tag{58}$$

We write the constant a_0 as a function of the wall surface impedance, defined as

$$\mathcal{R}_z = -\frac{E_z}{H_\theta}|_{r=b} \tag{59}$$

Using Eq. 37 and Eq. 41, for $r > a$ one gets

$$E_z(r) = j\frac{k_r}{\gamma}\phi = j\frac{k_r}{\gamma}\left[\frac{\rho I_0(k_r a)}{2\pi\epsilon_0}K_0(k_r r) + a_0 I_0(k_r r)\right] \tag{60}$$

$$Z_0 H_\theta(r) = -\beta\frac{d\phi}{dr} = \beta k_r\left[\frac{\rho I_0(k_r a)}{2\pi\epsilon_0}K_1(k_r r) - a_0 I_1(k_r r)\right] \tag{61}$$

Eqs. 59, 60 and 61 imply

$$a_0 = -\frac{\rho I_0(k_r a)}{2\pi\epsilon_0}\frac{K_0(k_r b) - j\beta\gamma\frac{\mathcal{R}_z}{Z_0}K_1(k_r b)}{I_0(k_r b) + j\beta\gamma\frac{\mathcal{R}_z}{Z_0}I_1(k_r b)} \ . \tag{62}$$

For an ideally conducting wall ($\mathcal{R}_z = 0$),

$$a_0^\infty = -\frac{\rho I_0(k_r a)}{2\pi\epsilon_0}\frac{K_0(k_r b)}{I_0(k_r b)} \ , \tag{63}$$

while the electric field is given by

$$E_z^\infty(r) = j\frac{k_r}{\gamma}\frac{\rho}{2\pi\epsilon_0}\left[G_0(r,a) - \frac{K_0(k_r b)}{I_0(k_r b)}I_0(k_r r)I_0(k_r a)\right] \tag{64}$$

in agreement with Eq. 4.1 of [3].

The resistive-wall impedance is produced by the electric field

$$E_z^\sigma(r) = E_z(r) - E_z^\infty(r) = -\frac{\rho I_0(k_r a)}{2\pi b\epsilon_0}\beta\frac{\mathcal{R}_z}{Z_0}\frac{1}{I_0(k_r b)\left[I_0(k_r b) + j\beta\gamma\frac{\mathcal{R}_z}{Z_0}I_1(k_r b)\right]}I_0(k_r r) \tag{65}$$

where the wronskian property of the Bessel functions, Eq. 54, was used. Note that the expressions of the electromagnetic field agree with the ones derived in [9].

2. *Impedance*

The monopole longitudinal impedance is

$$Z_0^{||\sigma} = -\frac{E_z^\sigma(r=0,a=0)}{\rho\beta c} = \frac{\mathcal{R}_z}{2\pi b}\frac{1}{I_0(k_r b)\left[I_0(k_r b) + j\beta\gamma\frac{\mathcal{R}_z}{Z_0}I_1(k_r b)\right]} \ . \tag{66}$$

The monopole transverse impedance is given by the derivative of the radial transverse force with respect to the affected particle displacement

$$Z_0^{\perp\sigma} = -\frac{\frac{\partial F_r}{\partial r}(r=0,a=0)}{jq\rho\beta c} = -\frac{\frac{\partial^2 E_z^\sigma}{\partial r^2}(r=0,a=0)}{k\rho\beta c} \ . \tag{67}$$

Since $I_0''(0) = \frac{1}{2}$,

$$Z_0^{\perp\sigma} = Z_0^{||\sigma}\frac{k}{2\gamma^2} \ . \tag{68}$$

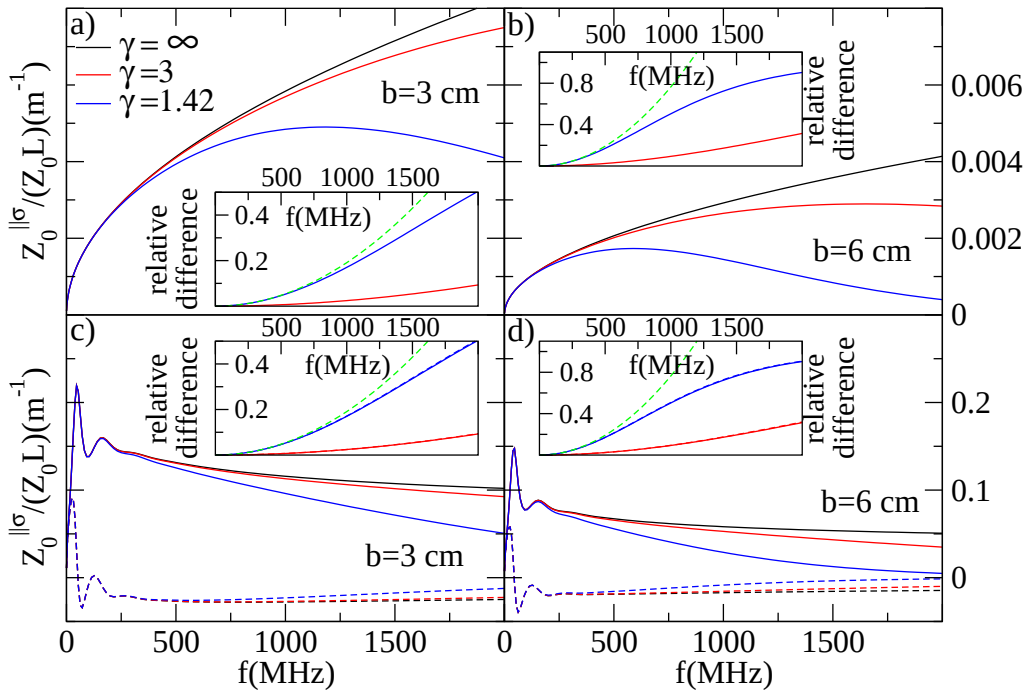

FIG. 1: Monopole longitudinal impedance for a metallic pipe (a and b) ($\sigma = 2.3 \times 10^6 \Omega^{-1} m^{-1}, \mu_r = 100$) and a laminated chamber (c and d). (The specific parameters are the same as in [12].) The solid (dashed) lines represent the real (imaginary) part of the impedance. For the metallic pipe, the imaginary and real parts of the impedance are equal in the frequency domain shown. The difference between the impedance and the ultrarelativistic impedance increases with increasing frequency and pipe radius. In the insets, the relative difference $\frac{Z_0^{||}(\gamma=\infty)-Z_0^{||\sigma}(\gamma)}{Z_0^{||}(\gamma=\infty)}$ is shown. The dashed green line represents the second-order correction to the ultrarelativistic limit for $\gamma = 1.42$, which is equal to $\frac{k_r^2 b^2}{2}$ according to Eq. 71. At large frequency the second-order approximation overestimates the impedance. At $1GHz$, for both metallic pipe and laminated chamber with radius $b = 3$ cm ($b = 6$ cm), we find $\approx 18\%$ ($\approx 50\%$) relative difference between the $\gamma = 1.42$ ultrarelativistic impedances.

3. *Comparison with previous calculations and discussion of the ultrarelativistic approximation*

In the frequency region of interest for beam dynamics $\frac{kb}{\gamma} \ll 1$, the small argument approximation for the Bessel functions, $I_0(x) \approx 1 + \frac{x^2}{4}$ and $I_1(x) \approx \frac{x}{2} + \frac{x^3}{16}$, can be used. Up to $\mathcal{O}(\gamma^{-2})$ the impedance can be written as

$$Z_0^{||\sigma} = \frac{\frac{\mathcal{R}_z}{2\pi b}}{1 + \frac{k^2 b^2}{2\gamma^2} + j\beta \frac{\mathcal{R}_z}{Z_0}\left(\frac{kb}{2} + \frac{3k^3 b^3}{16\gamma^2}\right)} . \tag{69}$$

In the ultrarelativistic limit, $\gamma \to \infty$, one gets

$$Z_0^{||\sigma} = \frac{\mathcal{R}_z}{2\pi b} \frac{1}{1 + j\frac{\mathcal{R}_z}{Z_0}\frac{kb}{2}} \tag{70}$$

in agreement with the ultrarelativistic derivation of [12, 20].

If only the first order terms is $\mathcal{R}_z$ are considered in Eq. 69,

$$Z_0^{||\sigma} \approx \frac{\mathcal{R}_z}{2\pi b} \frac{1}{1 + \frac{k^2 b^2}{2\gamma^2}} \approx \frac{\mathcal{R}_z}{2\pi b}\left(1 - \frac{k_r^2 b^2}{2}\right), \tag{71}$$

in agreement with [5]. Note that the impedance in this approximation exhibits poles at $k = \pm j\frac{\sqrt{2}\gamma}{b}$. This implies that the corresponding wake function is nonzero for positive z and decays as $\exp(-\frac{\sqrt{2}\gamma}{b}z)$.

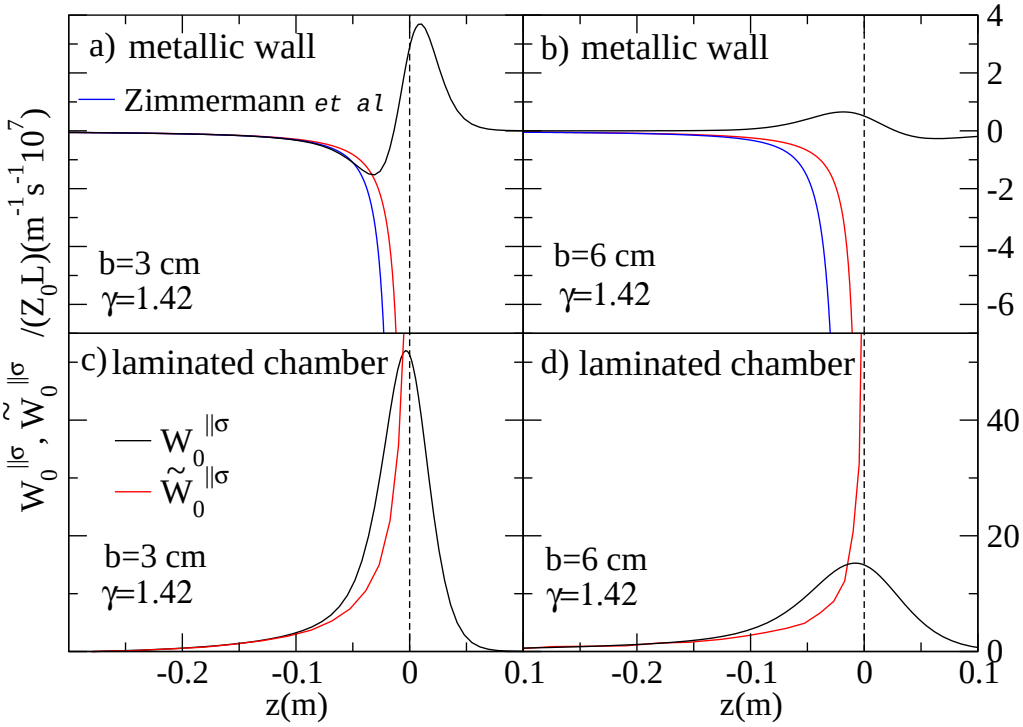

FIG. 2: Monopole longitudinal wake $W_0^{||\sigma}(z)$ (black) and the ultrarelativistic approximate wake $\tilde{W}_0^{||\sigma}(z)$(red) for metallic walls (a and b) and laminated chambers (c and d) for $\gamma = 1.42$. For the pipe radius of $b = 3$ cm ($b = 6$ cm) and at distances smaller than 0.1 m (0.2 m), both behind and in front of the source, the ultrarelativistic approximation fails to describe the wake. The approximation of Zimmermann *et al* for the metallic wall, (Eq. 64 in Ref [5], dashed blue) differs from our results.

In the following figures we show plots for two different types of vacuum chambers. One chamber type has a thick metallic wall with the well-known relation for the wall surface impedance, $\mathcal{R}_z = \frac{1+j}{\delta\sigma}$ [11, 20], where δ is the skin penetration depth and σ is the conductivity. The other chamber type has a laminated wall as studied in [12, 20]. Except for the chamber radius, all the others parameters are identical with those in [12]. The surface impedance in the laminated wall is qualitatively different and about two orders of magnitude larger than the metallic surface impedance; see Fig. 6 in [12].

In Fig. 1 we plot the longitudinal impedance $Z_0^{||\sigma}$ for three different values of γ: ultrarelativistic ($\gamma = \infty$), intermediate ($\gamma = 3$) and small ($\gamma = 1.42$), which corresponds to the Fermilab Booster injection energy. Circular chambers with two different radii, $b = 3$ cm and $b = 6$ cm, are considered. It can be seen (insets) that the difference between the impedance at finite γ and the ultrarelativistic approximation increases with both increasing frequency and pipe radius. This is expected from Eq. 71, which shows that the second order non-ultrarelativistic corrections are equal to $\frac{k_r^2 b^2}{2}$.

In Fig. 2 we plot the longitudinal wake $W_0^{||\sigma}(z)$, Eq. 4, and the ultrarelativistic approximate wake $\tilde{W}_0^{||\sigma}(z)$, Eq. 7, for $\gamma = 1.42$. The wake differs significantly from the ultrarelativistic approximation in the small-$|z|$ region ($|z| <\approx 0.1m - 0.2m$ in our example). This small-distance region is proportional to $\frac{b}{\gamma}$ as the imaginary part of the impedance poles implies. Unlike the ultrarelativistic case, the wake is nonzero in the small distance region ahead of the source. For small negative z the metallic pipe ultrarelativistic wake is larger and negative (attractive), displaying the familiar $|z|^{-\frac{3}{2}}$ behavior [19]. The true wake, however, is much smaller and becomes positive with decreasing $|z|$. For the laminated chambers with pipe radius of $b = 3$ cm ($b = 6$ cm), we find that the ultrarelativistic approximation strongly overestimates the wake function at distances smaller than $0.005m$ ($0.015m$) behind the source and underestimates it at at larger distances (but still in the small distance region). Note that the metallic wake behavior is also very different from the one predicted by Zimmermann *et al.* in [5]. They predict, by integrating the non-ultrarelativistic impedance truncated up to the second order in $k_r b$ and first order in $\mathcal{R}_z$, that $W_0^{||\sigma}(z)$ is proportional to $|z|^{-\frac{7}{2}}$ at small z. However this approximation for the impedance is not valid at large frequency where both $k_r b$ and $\mathcal{R}_z \propto \sqrt{\omega}$ are large.

The monopole transverse impedance, Eq. 68, vanishes in the ultrarelativistic limit. The finite-γ monopole transverse

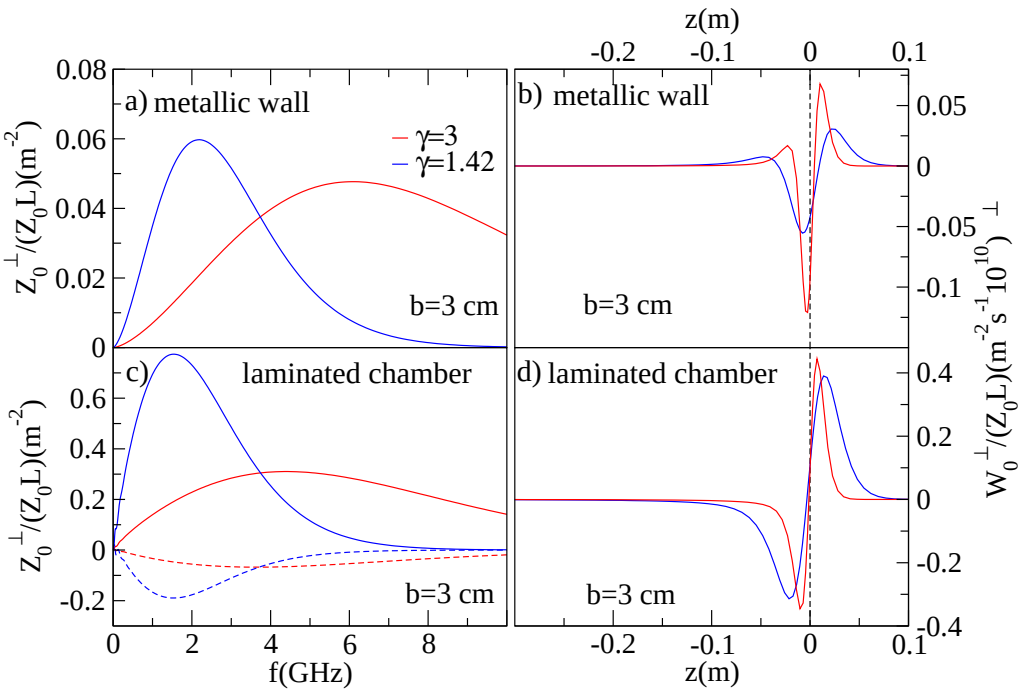

FIG. 3: Transverse monopole impedance $Z_0^{\sigma\perp}$ and the corresponding wake $W_0^{\sigma\perp}$ for $\gamma = 3$ (red) and $\gamma = 1.42$ (blue). For a metallic wall the real (solid line) and imaginary (dashed line) parts of the impedance are approximately the same. The impedance shows a wide peak at frequency of order of several GHz. With decreasing γ the peak magnitude increases and shifts to smaller frequency. The wake function is noticeable both for negative and positive values of z, in the small distance region proportional to $\frac{b}{\gamma}$, although it is about one order of magnitude smaller than the dipole transverse wake.

impedance and the corresponding wake are displayed in Fig. 3 for both metallic and laminated chambers with radius $b = 3$ cm. The impedance shows a wide peak at a frequency of several GHz. The peak increases and shifts to smaller frequency with decreasing γ. The wake function is significant in the small distance region, in our example $<\approx 0.1m$ ($<\approx 0.05m$) for $\gamma = 1.42$ ($\gamma = 3$), for both positive and negative values of z. For small γ, compared with the dipole transverse impedance (discussed in the next section), the monopole transverse impedance magnitude is about two orders of magnitude smaller but spreads to much higher frequency. The monopole transverse wake is about one order of magnitude smaller than the dipole transverse wake in the small distance region.

B. Dipole channel, $m = 1$

1. *Electromagnetic field solution*

In order to calculate the vector potential, we define, as in in Ref. [5],

$$A_+ = A_r + A_\theta \tag{72}$$
$$A_- = A_r - A_\theta \ . \tag{73}$$

The equations 29 and 30 imply

$$\frac{d^2A_+}{dr^2} + \frac{1}{r}\frac{dA_+}{dr} - (\frac{2}{r^2} + k_r^2)A_+ = 0 \tag{74}$$
$$\frac{d^2A_-}{dr^2} + \frac{1}{r}\frac{dA_-}{dr} - k_r^2 A_- = 0 \tag{75}$$

with solutions

$$A_+ = q_+ I_2(k_r r) \tag{76}$$
$$A_- = q_- I_0(k_r r) \ . \tag{77}$$

A gauge transformation with

$$\chi \;=\; vI_1(k_r r) \tag{78}$$

with $v = \frac{q_+ + q_-}{2k_r}$ will make $q_+ = -q_- \equiv q_1$. Therefore one has

$$A_r = q_1(I_2(k_r r) - I_0(k_r r)) \tag{79}$$
$$A_\theta = q_1(I_2(k_r r) + I_0(k_r r)) \ . \tag{80}$$

The Lorentz condition, Eq. 32,

$$q_1 k_r \left[I_2'(k_r r) - I_0'(k_r r)\right] + \frac{2q_1}{r} I_2(k_r r) - jk\left(A_z - \frac{\beta}{c}\phi\right) = 0 \ , \tag{81}$$

implies

$$A_z = \frac{\beta}{c}\phi \ , \tag{82}$$

as in the $m = 0$ case. Here $I_2'(x) - I_0'(x) = -\frac{2}{x} I_2(x)$ was used.

Taking into account that the solution to the equation

$$\frac{d^2 G_1}{dr^2} + \frac{1}{r}\frac{dG_1}{dr} - (\frac{1}{r^2} + k_r^2)G_1 = -\frac{\delta(r-a)}{a} \tag{83}$$

is

$$G_1(r,a) = \begin{cases} K_1(k_r a) I_1(k_r r), & r < a \\ I_1(k_r a) K_1(k_r r), & r > a \ , \end{cases} \tag{84}$$

the potentials become

$$\phi(r) \;=\; \frac{\rho}{\pi\epsilon_0} G_1(r,a) + a_1 I_1(k_r r) \tag{85}$$
$$A_r \;=\; q_1\left(I_2(k_r r) - I_0(k_r r)\right) = -\frac{2q_1}{k_r r} I_1(k_r r) \tag{86}$$
$$A_\theta \;=\; q_1\left(I_2(k_r r) + I_0(k_r r)\right) = 2q_1 I_1'(k_r r) \tag{87}$$
$$A_z \;=\; \frac{\rho\beta}{\pi\epsilon_0 c} G_1(r,a) + \frac{\beta}{c} a_1 I_1(k_r r) \tag{88}$$

The electromagnetic field components are

$$E_z \;=\; j\frac{k_r}{\gamma}\left(\frac{\rho}{\pi\epsilon_0} G_1(r,a) + a_1 I_1(k_r r)\right) \tag{89}$$
$$E_\theta \;=\; \frac{\rho}{\pi\epsilon_0 r} G_1(r,a) + \frac{a_1}{r} I_1(k_r r) - 2jq_1 k\beta c I_1'(k_r r) \tag{90}$$
$$E_r \;=\; -\frac{\rho}{\pi\epsilon_0}\frac{dG_1}{dr}(r,a) - a_1 k_r I_1'(k_r r) + 2jq_1\gamma\beta c\frac{I_1(k_r r)}{r} \tag{91}$$
$$Z_0 H_z \;=\; 2q_1 c k_r I_1(k_r r) \tag{92}$$
$$Z_0 H_\theta \;=\; -\frac{\beta\rho}{\pi\epsilon_0}\frac{dG_1}{dr}(r,a) - a_1 k_r \beta I_1'(k_r r) + 2jq_1\gamma c\frac{I_1(k_r r)}{r} \tag{93}$$
$$Z_0 H_r \;=\; -\frac{\beta\rho}{\pi\epsilon_0 r} G_1(r,a) - \frac{\beta}{r} a_1 I_1(k_r r) + 2jq_1 k c I_1'(k_r r) \ . \tag{94}$$

The next step is to determine the constant a_1. As in the monopole case we want to write it as function of the wall surface impedances, defined as

$$\mathcal{R}_z = -\frac{E_z}{H_\theta}|_{r=b} \tag{95}$$
$$\mathcal{R}_\theta = \frac{E_\theta}{H_z}|_{r=b} \ . \tag{96}$$

Employing Eqs. 89, 90, 92, 93, 95 and 96 we get a system of two linear equations

$$a_1 k_r \left(j\frac{I_1(k_r b)}{\gamma} - \beta\frac{\mathcal{R}_z}{Z_0} I_1'(k_r b)\right) + 2jq_1\gamma c\frac{\mathcal{R}_z}{Z_0}\frac{I_1(k_r b)}{b} = k_r \frac{\rho I_1(k_r a)}{\pi\epsilon_0}\left(\beta\frac{\mathcal{R}_z}{Z_0}K_1'(k_r b) - j\frac{K_1(k_r b)}{\gamma}\right) \tag{97}$$

$$a_1\frac{I_1(k_r b)}{b} - 2q_1(jk\beta c I_1'(k_r b) + ck_r\frac{\mathcal{R}_\theta}{Z_0}I_1(k_r b)) = -\frac{\rho I_1(k_r a)}{\pi\epsilon_0 b}K_1(k_r b)\ . \tag{98}$$

It follows that

$$a_1 = -\frac{\rho I_1(k_r a)}{\pi\epsilon_0}\frac{\left[\frac{K_1}{I_1} + \frac{\mathcal{R}_z\mathcal{R}_\theta}{Z_0^2}\frac{K_1'}{I_1'} - j\gamma\frac{\mathcal{R}_z}{\beta Z_0}\left(\frac{1}{k_r^2 b^2}\frac{K_1}{I_1'} - \beta^2\frac{K_1'}{I_1}\right) - j\frac{\mathcal{R}_\theta}{\beta Z_0\gamma}\frac{K_1}{I_1'}\right]}{\left[1 + \frac{\mathcal{R}_z\mathcal{R}_\theta}{Z_0^2} - j\gamma\frac{\mathcal{R}_z}{\beta Z_0}\left(\frac{1}{k_r^2 b^2}\frac{I_1}{I_1'} - \beta^2\frac{I_1'}{I_1}\right) - j\frac{\mathcal{R}_\theta}{Z_0\beta\gamma}\frac{I_1}{I_1'}\right]} \tag{99}$$

where the Bessel functions are evaluated at $k_r b$, i.e. $I_1 \equiv I_1(k_r b)$ and $K_1 \equiv K_1(k_r b)$.

For ideally conducting walls, i.e. when $\mathcal{R}_z = \mathcal{R}_\theta = 0$, one gets

$$E_z^\infty = j\frac{k_r}{\gamma}\frac{\rho}{\pi\epsilon_0}\left(G_1(r,a) - \frac{K_1(k_r b)}{I_1(k_r b)}I_1(k_r a)I_1(k_r r)\right)\ . \tag{100}$$

The wall finite-conductivity contribution to the electric field is

$$E_z^\sigma = E_z - E_z^\infty = \frac{\rho k_r I_1(k_r a)I_1(k_r r)}{\pi\epsilon_0}\frac{\beta\frac{\mathcal{R}_z}{Z_0}\left(\frac{K_1'}{I_1} - \frac{K_1 I_1'}{I_1^2}\right) + \frac{\mathcal{R}_z\mathcal{R}_\theta}{Z_0^2}\left(\frac{K_1'}{I_1'} - \frac{K_1}{I_1}\right)}{\left[1 - j\gamma\frac{\mathcal{R}_z}{\beta Z_0}\left(\frac{1}{k_r^2 b^2}\frac{I_1}{I_1'} - \beta^2\frac{I_1'}{I_1}\right) + \frac{\mathcal{R}_z\mathcal{R}_\theta}{Z_0^2} - j\frac{\mathcal{R}_\theta}{Z_0\beta\gamma}\frac{I_1}{I_1'}\right]}\ . \tag{101}$$

2. *Impedance*

According to Eqs. 22 and 43 and using $I_1'(0) = \frac{1}{2}$, the transverse impedance reads

$$Z_1^{\perp\sigma} = -\frac{\frac{\partial^2 E_z}{\partial a\partial r}(r=0,a=0)}{\rho\beta c k} = -\frac{k_r^2}{4\pi\gamma}\frac{\mathcal{R}_z\left(\frac{K_1'}{I_1} - \frac{K_1 I_1'}{I_1^2}\right) + \frac{\mathcal{R}_z\mathcal{R}_\theta}{\beta Z_0}\left(\frac{K_1'}{I_1'} - \frac{K_1}{I_1}\right)}{\left[1 - j\gamma\frac{\mathcal{R}_z}{\beta Z_0}\left(\frac{1}{k_r^2 b^2}\frac{I_1}{I_1'} - \beta^2\frac{I_1'}{I_1}\right) + \frac{\mathcal{R}_z\mathcal{R}_\theta}{Z_0^2} - j\frac{\mathcal{R}_\theta}{Z_0\beta\gamma}\frac{I_1}{I_1'}\right]}\ . \tag{102}$$

Note that the dipole longitudinal impedance (which effects are of second order in the particles displacement), is related to the transverse impedance

$$Z_1^{||\sigma} = -\frac{\frac{\partial^2 E_z}{\partial a\partial r}(r=0,a=0)}{\rho\beta c} = Z_1^{\perp\sigma}k\ . \tag{103}$$

Because $\frac{\partial F_{r,\theta}}{\partial r}(a=0,r=0) = 0$, the dipole channel does not yield transverse wakes acting on the affected particle displacement.

3. *Comparison with previous calculations and discussion of the ultrarelativistic approximation*

Using the small argument approximation of the Bessel functions

$$I_1(x) \approx \frac{x}{2}\left(1 + \frac{x^2}{8} + \frac{x^4}{192}\right) \tag{104}$$

$$I_1'(x) \approx \frac{1}{2}\left(1 + \frac{3x^2}{8} + \frac{5x^4}{192}\right) \tag{105}$$

$$\frac{I_1(x)}{I_1'(x)} \approx x\left(1 - \frac{x^2}{4} + \frac{59x^4}{192}\right) \tag{106}$$

$$\frac{I_1'(x)}{I_1(x)} \approx \frac{1}{x}\left(1 + \frac{x^2}{4} + \frac{19x^4}{192}\right) \tag{107}$$

$$K_1(x) \approx \frac{1}{x} \tag{108}$$

$$K_1'(x) \approx -\frac{1}{x^2} \tag{109}$$

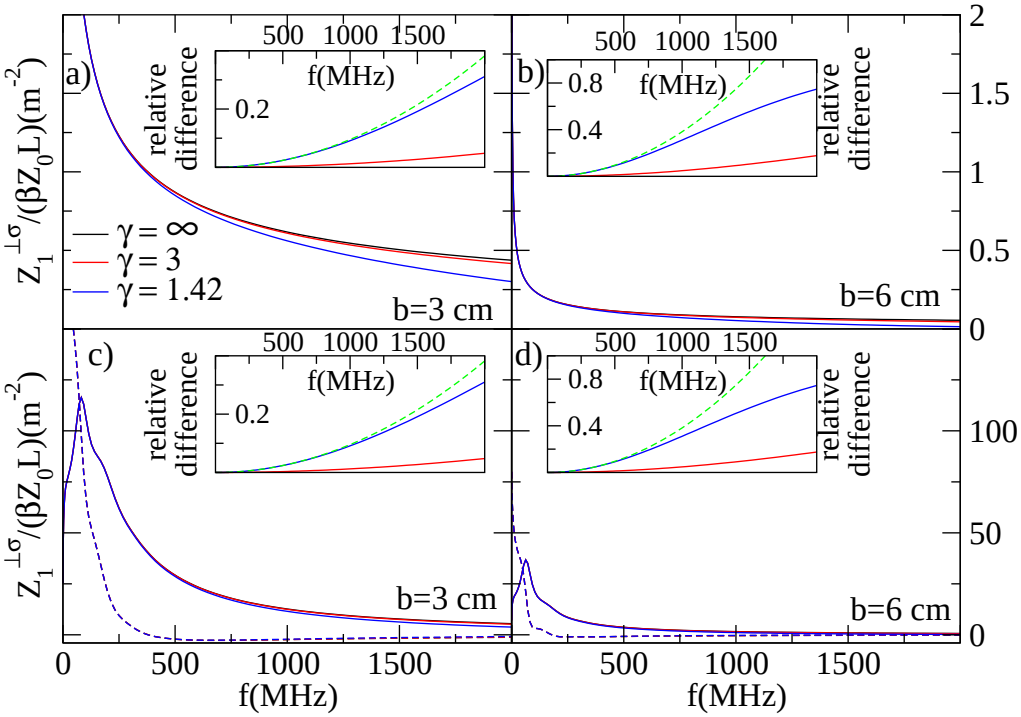

FIG. 4: Dipole transverse impedance divided by β for metallic (a and b) and laminated (c and d) chambers. The solid (dashed) lines represent the real (imaginary) part of the impedance. For the metallic pipe the imaginary and the real part of the impedance are equal in the frequency domain shown. The difference between the impedance and the ultrarelativistic impedance increases with increasing frequency and pipe radius. In the insets, the relative difference $\frac{Z_1^{\perp}(\gamma=\infty)-Z_1^{\perp\sigma}(\gamma)/\beta}{Z_1^{\perp}(\gamma=\infty)}$ is shown. The dashed green line represents the second order correction to the ultrarelativistic limit for $\gamma = 1.42$, equal to $\frac{k_r^2 b^2}{4}$ according to Eq. 112. At large frequency the second-order approximation overestimates the impedance. At $1GHz$, for both the metallic pipe and the laminated chamber with radius $b = 3$ cm ($b = 6$ cm) we find $\approx 9\%$ ($\approx 25\%$) relative difference between the $\gamma = 1.42$ and ultrarelativistic impedances.

up to $\mathcal{O}(\gamma^{-2})$, the dipole impedance is

$$Z_1^{||\sigma} = Z_1^{\perp\sigma} k = \frac{\frac{\mathcal{R}_z}{\pi b^3} - \frac{\mathcal{R}_z k^2}{4\pi b\gamma^2} + \frac{\mathcal{R}_z \mathcal{R}_\theta}{\beta Z_0}\frac{k}{\pi b^2 \gamma}}{1 - j\frac{\mathcal{R}_z}{\beta Z_0}\left(\frac{1}{kb} - \frac{kb(1+\beta^2)}{4}\right) + \frac{\mathcal{R}_z\mathcal{R}_\theta}{Z_0^2} - j\frac{\mathcal{R}_z}{Z_0\beta}\frac{k^3 b^3(59+19\beta^2)}{192\gamma^2} - j\frac{\mathcal{R}_\theta}{Z_0\beta}\frac{kb}{\gamma^2}} \,. \tag{110}$$

In the ultrarelativistic limit

$$Z_1^{||\sigma} = Z_1^{\perp\sigma} k = \frac{\frac{\mathcal{R}_z}{\pi b^3}}{1 - j\frac{\mathcal{R}_z}{Z_0}\left(\frac{1}{kb} - \frac{kb}{2}\right) + \frac{\mathcal{R}_z\mathcal{R}_\theta}{Z_0^2}} \,, \tag{111}$$

in agreement with [12].

Up to first order in the wall surface impedance and to second order in γ^{-1}

$$Z_1^{\perp\sigma} = \frac{\mathcal{R}_z}{k\pi b^3} - \frac{\mathcal{R}_z k}{4\pi b\gamma^2} = \frac{\mathcal{R}_z}{k\pi b^3}\left(1 - \frac{k_r^2 b^2}{4}\right), \tag{112}$$

in agreement with [5].

In Fig. 4 we plot the dipole transverse impedance for the metallic and the laminated chambers. For comparison with the ultrarelativistic case the transverse impedance is normalized by a factor of β since it is proportional to $F_r \propto k^{-1} \propto \beta$ (see Eq. 43). Similar conclusions with the ones found for the longitudinal monopole impedance can be drawn. The difference between the impedance and the ultrarelativistic approximation increases with both increasing

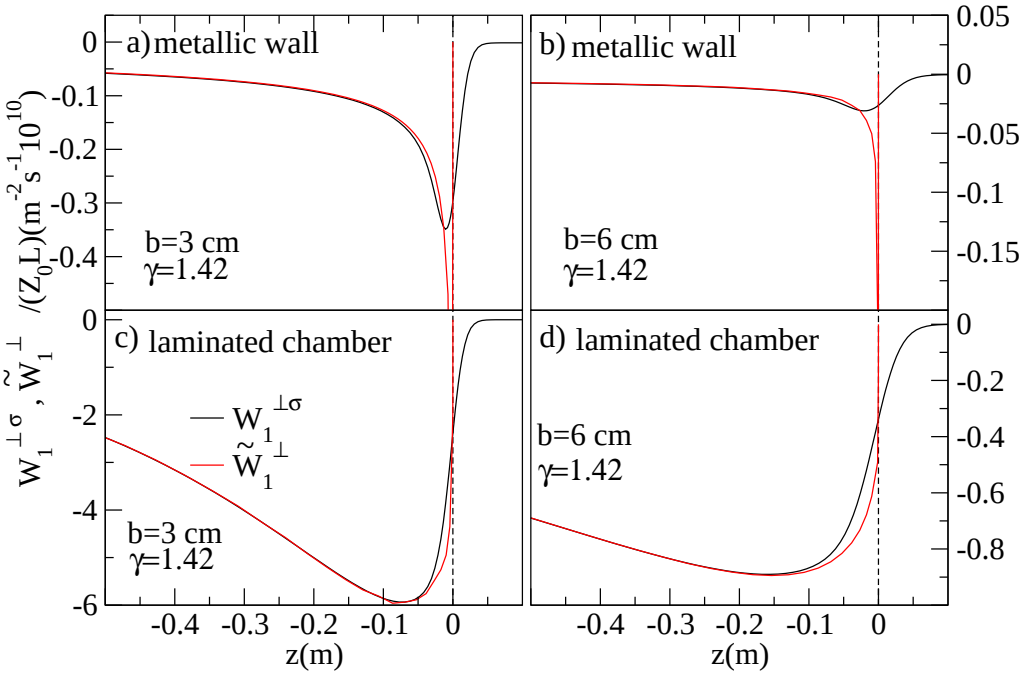

FIG. 5: Transverse wake $W_1^{\perp\sigma}$ (black) and the ultrarelativistic approximation $\tilde{W}_1^{\perp}$ (red) for metallic wall (a and b) and laminated (c and d) chambers, for $\gamma = 1.42$. The ultrarelativistic approximation is not valid in the small distance region.

the frequency and the pipe radius. The second-order approximation. which predicts the relative difference to be $\frac{k_r^2 b^2}{4}$, Eq. 112, overestimates the impedance at large frequency.

In Fig. 5 the transverse wake, $W_1^{\perp\sigma}$, and the ultrarelativistic approximation $\tilde{W}_1^{\perp}$ are shown for $\gamma = 1.42$. Significant differences between the two wakes can be noticed at small distances. At small and negative z, $|z| <\approx 0.1$ m in our example, the metallic ultrarelativistic wake displays the expected $|z|^{-0.5}$ behavior [19], being large and negative. However, in this region the real metallic wake is much smaller. The laminated wake also has a smaller magnitude than the ultrarelativistic approximation in the small distance region behind the source. Ahead of the source, for $z <\approx 0.05$ m, both metallic and laminated wakes are nonzero and decrease rapidly with increasing z.

IV. CONCLUSIONS

We calculated general expressions for the longitudinal and the transverse impedances in circular chambers, writing them as function of the wall surface impedance. The equations are valid for all types of walls as long as the wall surface impedance can be defined. The wall's electrical properties are contained implicitly in the surface impedance. The advantage of this approach is that the problems related to the wall properties are now separated from the impedance calculation and can be addressed separately for each specific wall type.

We numerically calculated the resistive-wall wakes for the metallic and the laminated chambers and discussed the validity of the ultrarelativistic approximation for the non-ultrarelativistic beams. We found that the ultrarelativistic approximation fails to describe the wake effects at distances smaller than ≈ 0.1 m for chambers with radius of a few centimeters at small and intermediate γ. Unlike the ultrarelativistic wake, which vanishes in front of the source, the non-ultrarelativistic case includes a repulsive wake ahead of the source, which is a consequence of the fact that the electromagnetic field propagates faster than the source. In the small distance region behind the source, the ultrarelativistic approximation strongly overestimates the wake fields. Aside from the familiar transverse wake term which couples to the source particle displacement, the non-ultrarelativistic beams in circular chambers are characterized by a transverse wake which couples with the displacement of the affected particle. This transverse wake term is of order $\mathcal{O}(\gamma^{-2})$ and acts in the small distance region both ahead and behind the source.

Our results imply that non-ultrarelativistic beam simulations using both space-charge and ultrarelativistic wakes introduce strong artificial collective interactions at small distance. The artificial effects are expected to affect the stability of short beams, of order of 0.1 m, most strongly. However other quantities such as beam size, emittance,

phase space properties, tunes, are expected to be affected even for long beams. Investigation of the spurious effects introduced by the ultrarelativistic wakes in non-ultrarelativistic beam simulations will be presented in future work.

V. ACKNOWLEDGMENTS

This work was supported by the United States Department of Energy under contract DE-AC02-07CH11359, the ComPASS project, funded through the Scientific Discovery through Advanced Computing program in the DOE Office of High Energy Physics, and NSF grant 0237162. This research used resources of the National Energy Research Scientific Computing Center, which is supported by the Office of Science of the U.S. Department of Energy under Contract No. DE-AC02-05CH11231, as well as resources of the Argonne Leadership Computing Facility at Argonne National Laboratory, which is supported by the Office of Science of the U.S. Department of Energy under contract DE-AC02-06CH11357.

[1] S. A. Heifets and S. A. Kheifets, Rev. of Mod. Phys. **63**, 631 (1991).
[2] B Zotter and S. A. Kheifets, "Impedances and Wakes in High-Energy Particle Accelerators", World Scientific Publishing, (1998).
[3] R. Gluckstern, CERN Report No. 2000-011, 2000.
[4] A. M. Al-Khateeb, O. Boine-Frankenheim, I. Hofmann and Giovanni Rumolo, Phys. Rev. E **63**, 026503 (2001).
[5] F. Zimmermann and K. Oide, PRST-AB **7**, 044201 (2004).
[6] A. M. Al-Khateeb, O. Boine-Frankenheim, R. W. Hasse, and I. Hofmann, Phys. Rev. E **71**, 026501 (2005).
[7] A. M. Al-Khateeb, R. W. Hasse, O. Boine-Frankenheim, W. M. Daqa, and I. Hofmann, Phys. Rev. ST Accel. Beams **10**, 064401 (2007).
[8] N. Wang and Q. Qin, Phys. Rev. ST Accel. Beams **10**, 111003 (2007).
[9] H. Hahn, Phys. Rev. ST Accel. Beams 13, 012002 (2010).
[10] K. Y. Ng, Fermilab Report FN-443 (1987).
[11] J. D. Jackson, Classical Electrodynamics, 3rd edition, John Wiley & Sons, Inc. New York (1999).
[12] A. Macridin, P. Spentzouris, J. Amundson L. Spentzouris and D. McCarron, Phys. Rev. ST Accel. Beams **14**, 061003 (2011).
[13] J. Amundson, P. Spentzouris, J. Qiang, and R. Ryne, J. Comput. Phys. 211, 229 (2006).
[14] J. Qiang, R. D. Ryne, S. Habib and V. Decyk, J. Comp. Phys. 163, 434 (2000).
[15] J. A. Holmes, V. Danilov, J. Galambos, A. Shishlo, S. Cousineau, W. Chou, L. Michelotti, J.F. Ostiguy, and J. Wei, AIP Conf. Proc. **642**, (2002).
[16] A. Chao, S. Heifets and Bruno Zotter, Phys. Rev. ST AB **5**, 111001 (2002).
[17] S. Heifets, A. Wagner, B. Zotter, SLAC/AP110 (1998).
[18] A. Burov and V. Lebedev, Fermilab Report, FERMILAB-CONF-02-101-T, 2002.
[19] A. Chao, "Physics of Collective Beam Instabilities in High Energy Accelerators," John Wiley & Sons, Inc. New York (1993).
[20] K. Y. Ng, Fermilab Report FN-0744 (2004).